RESEARCH ARTICLE

The evolution of light and vertical mixing across a phytoplankton ice-edge bloom

Achim Randelhoff[*,†], Laurent Oziel[*,†,‡], Philippe Massicotte[*,†], Guislain Bécu[*,†], Martí Galí[*,†], Léo Lacour[*,†], Dany Dumont[§], Anda Vladoiu[‖], Claudie Marec[*,†,¶], Flavienne Bruyant[*,†], Marie-Noëlle Houssais[‖], Jean-Éric Tremblay[*,†], Gabrièle Deslongchamps[*,†] and Marcel Babin[*,†]

During summer, phytoplankton can bloom in the Arctic Ocean, both in open water and under ice, often strongly linked to the retreating ice edge. There, the surface ocean responds to steep lateral gradients in ice melt, mixing, and light input, shaping the Arctic ecosystem in unique ways not found in other regions of the world ocean. In 2016, we sampled a high-resolution grid of 135 hydrographic stations in Baffin Bay as part of the Green Edge project to study the ice-edge bloom, including turbulent vertical mixing, the under-ice light field, concentrations of inorganic nutrients, and phytoplankton biomass. We found pronounced differences between an Atlantic sector dominated by the warm West Greenland Current and an Arctic sector with surface waters originating from the Canadian archipelago. Winter overturning and thus nutrient replenishment was hampered by strong haline stratification in the Arctic domain, whereas close to the West Greenland shelf, weak stratification permitted winter mixing with high-nitrate Atlantic-derived waters. Using a space-for-time approach, we linked upper ocean dynamics to the phytoplankton bloom trailing the retreating ice edge. In a band of 60 km (or 15 days) around the ice edge, the upper ocean was especially affected by a freshened surface layer. Light climate, as evidenced by deep 0.415 mol $m^{-2} d^{-1}$ isolumes, and vertical mixing, as quantified by shallow mixing layer depths, should have permitted significant net phytoplankton growth more than 100 km into the pack ice at ice concentrations close to 100%. Yet, under-ice biomass was relatively low at 20 mg chlorophyll-a m^{-2} and depth-integrated total chlorophyll-a (0–80 m) peaked at an average value of 75 mg chlorophyll-a m^{-2} only around 10 days after ice retreat. This phenological peak may hence have been the delayed result of much earlier bloom initiation and demonstrates the importance of temporal dynamics for constraints of Arctic marine primary production.

Keywords: Arctic; Phytoplankton; Ice edge; Spring bloom; Light; Turbulence

Introduction

Every year in summer, the Arctic ice edge retreats hundreds of kilometers from its mid-March maximum extent to its mid-September minimal extent. The retreat is not evenly distributed: in some places like Fram Strait it lin-

* Takuvik Joint International Laboratory, Laval University (Canada), CNRS, FR

† Département de biologie et Québec-Océan, Université Laval, Québec, CA

‡ Remote Sensing Unit, Bedford Institute of Oceanography, Fisheries and Oceans Canada, Dartmouth, Nova Scotia, CA

§ Institut des sciences de la mer de Rimouski, Université du Québec à Rimouski, CA

‖ Sorbonne Université (UPMC, Paris 6)/CNRS/UPMC/IRD/MNHN, Laboratoire d'Océanographie et du Climat (LOCEAN), Institut Pierre Simon Laplace, Paris, FR

¶ Laboratoire d'Océanographie Physique et Spatiale (LOPS), CNRS/IFREMER/IRD/UBO, Plouzane, FR

Corresponding author: Achim Randelhoff (achim.randelhoff@takuvik.ulaval.ca)

gers for most of the year because of dominant ice-drift patterns; in others, such as off Siberia, it retreats rapidly from the shallow shelves into the central Arctic basin (Steele and Ermold, 2015). Phytoplankton blooms trailing these ice edges are a dominant feature in the Arctic Ocean (Perrette et al., 2011).

The overall phenology of these blooms is now fairly well documented (see, e.g., Sakshaug, 2004; Carmack and Wassmann, 2006; Wassmann and Reigstad, 2011). With the return of the sun in Arctic spring, ice melts quickly in the marginal ice zone (MIZ). Around the ice edge, pelagic phytoplankton can bloom until either nutrients are depleted, which seems to be the case in most scenarios studied in the Arctic (e.g., Sakshaug, 2004), or until the grazing pressure becomes too high as zooplankton resurface from their deeper overwintering habitat to feed and reproduce. During the bloom, primary and secondary producers awaken rapidly, consuming the available inorganic nutrients and eventually switching from an autotrophic to a heterotrophic or mixotrophic food web, concurrent with the development

of a subsurface chlorophyll-a (chl-a) maximum as a compromise between nutrient and light availability.

An important recognition in the last two decades has been that even small leads, cracks, melt ponds or thin ice without snow can in fact let enough light pass to permit pelagic blooms in ice-covered areas (e.g., Fortier et al., 2002; Mundy et al., 2009; Arrigo et al., 2014; Lowry et al., 2014; Assmy et al., 2017). Whether or not these blooms are more vigorous than the ones in open water depends strongly on the light transmittance and nutrient availability (Arrigo et al., 2014; Assmy et al., 2017), but in general they will consume nutrients, which modifies the dissolved nutrient pool and potentially alters the community composition later in the season and downstream of the MIZ (Sakshaug, 2004).

There are a number of hypotheses about the conditions necessary or sufficient for triggering the phytoplankton spring bloom (e.g., Behrenfeld and Boss, 2017, and references therein), at least as far as the global ocean goes. These hypotheses usually relate to critical levels or penetration depths of light, turbulence or distribution of grazers (see also e.g. Behrenfeld, 2010; Franks, 2015). All of these factors are interrelated by vertical mixing of plankton within (and potentially out of) the photic zone. Crucially, mixing is suppressed during and after the winter-spring restratification of the upper ocean, and in the MIZ due to strong ice melt (McPhee and Kantha, 1989; Randelhoff et al., 2017; Cole et al., 2018).

In the Arctic Ocean in particular, however, ice melt and ice retreat are often strongly correlated when newly exposed water is rapidly heated by the sun in spring and summer (Steele and Ermold, 2015), and so both stratification and increased light input are temporally linked to the spring bloom. The picture becomes less clear the more closely one examines the problem, as the case of under-ice blooms has demonstrated. Does the onset of these blooms rely on the developing stratification that reduces the intensity and depth of vertical mixing below an ice cover that is just starting to melt, or is the light that passes through the optically thinner ice, whether through leads or a melting snow cover, sufficient alone? Part of the answer certainly requires detailed physiological studies of the blooming phytoplankton species, but the vertical extents of light penetration and mixing, in conjunction with nutrient loading, can inform of important constraints on the overall occurrence of ice-edge blooms.

Baffin Bay replicates the large-scale gradients of the pan-arctic regime, with a more temperate current from the North Atlantic and a colder one of Arctic origin (e.g., Tang et al., 2004; Curry et al., 2014). The Arctic current, being derived from Pacific water, is light enough to pass over the shallow sills of the Canadian Archipelago north of Baffin Bay, flowing southward along the western shelf and becoming progressively diluted (Fissel et al., 1982). The West Greenland Current carries mostly nutrient-richer Atlantic water, and a smaller amount of Arctic water on top originating in Fram Strait and carried south by the East Greenland current (Torres-Valdés et al., 2013). The West Greenland Current is therefore much saltier and heavier; it cannot pass over the sills in the north and recirculates south after subducting under (and mixing with) the Arctic current (**Figure 1**; see also Münchow et al., 2015).

In addition, the ice edge in Baffin Bay usually retreats evenly and features a predictable spring bloom (Perrette
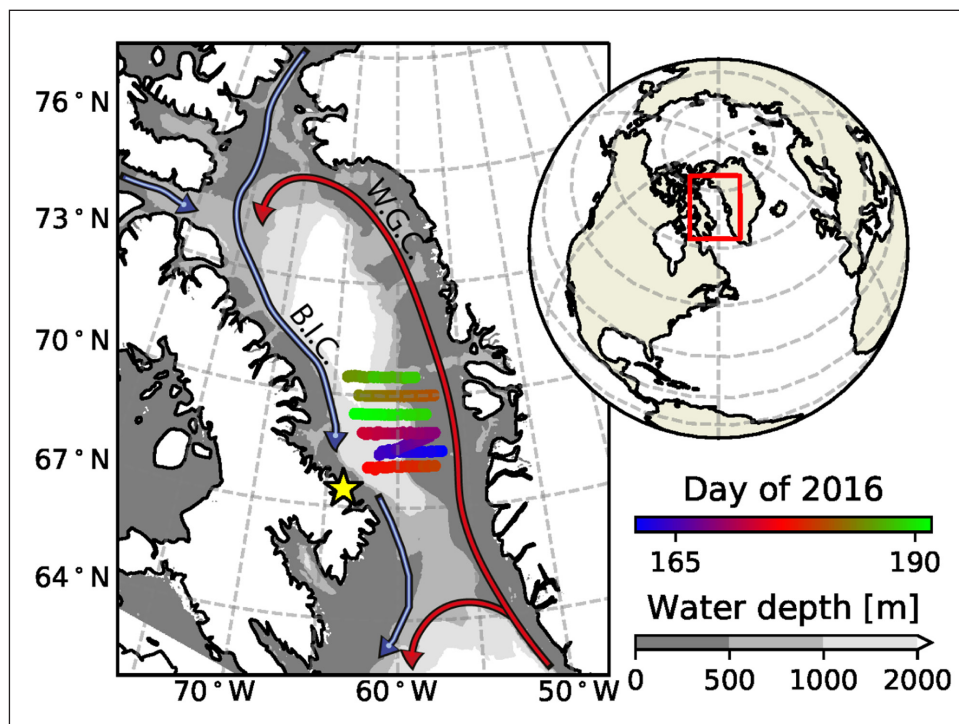
Figure 1: Map of Baffin Bay. Baffin Bay, located between Baffin Island, Greenland, and the Arctic and North Atlantic oceans. Sampling locations are colour-coded for doy, the "(decimal) day of the year" (doy 160 = 8 June, doy 190 = 8 July); bathymetry is indicated as greyscale shading (Jakobsson et al., 2012). The yellow star indicates the location of the ice camps in 2015 and 2016 (Oziel et al., 2019). The red arrow represents the Atlantic-derived West Greenland Current; the blue one the Arctic-derived Baffin Island Current. DOI: https://doi.org/10.1525/elementa.357.f1

et al., 2011). Baffin Bay is thus a good model system to study the roles of biogeochemistry, hydrography and optical properties in and around Arctic ice-edge blooms. The data collected during the Green Edge campaign (see Special Feature overview) showcase the spatial variation along east–west gradients in the large-scale hydrographic background as well as how mixing, stratification, and light climate influence nutrient and phytoplankton dynamics.

Methods
The CCGS Amundsen 2016 expedition and Green Edge project in Baffin Bay
Sampling aboard the CCGS *Amundsen* during the Green Edge campaign extended from 09 June to 10 July 2016. The sampling locations were distributed along seven longitudinal transects across the ice edge, each at a different latitude (**Figure 2**). The total data set comprises around 135 sampling stations. For an impression of the general region, additional maps can be found in the supplemental material (Figures S1.1–S1.4).

Hydrographic sampling
At each hydrographic station, vertical profiles of water column properties were made using a Conductivity-Temperature-Depth sensor system (CTD, Seabird SBE-911 plus), installed onboard the CCGS *Amundsen* which also included a Seapoint SCF Fluorometer for detection of chl-a, and a WetLabs C-Star transmissometer to measure beam attenuation as an indicator of biomass. In total, over all 135 sampling stations, 200 CTD casts were conducted. CTD data processing was done by the Amundsen Science Team following standard procedures (Guillot, 2016).
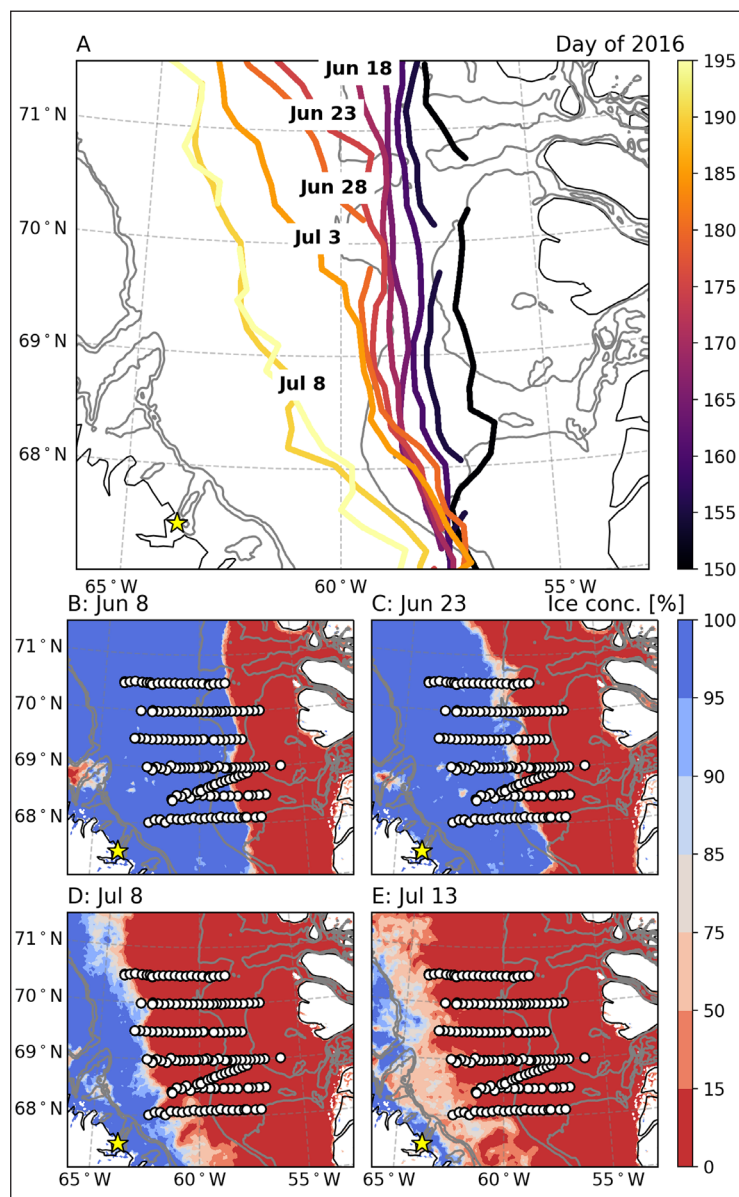
Figure 2: Evolution of the ice cover through summer. A: Location of the ice edge at a given doy. **B, C, D, E:** Ice concentrations at doy 160, 175, 190 and 195, respectively. Note the non-linear color scale for the ice concentration. For reference, panels B to E also show the hydrographic station grid. Grey lines indicate isobaths at 250 and 500 m; see Figure 1 for more information on the bathymetry. The yellow star indicates the location of the 2015/2016 ice camps. DOI: https://doi.org/10.1525/elementa.357.f2

For the purpose of this study, temperatures are always given as conservative temperature, T_C, defined according to the TEOS-10 standard (IOC, SCOR, IAPSO, 2010); the same applies to the use of S_A for absolute salinity.

The maximum temperature of each vertical profile is a reliable tracer for water masses of Atlantic origin (Tang et al., 2004). It was extracted for each hydrographic station, making sure that the CTD profile had passed through the core by requiring that temperature was decreasing below the maximum (not all profiles were sampled deeper than that maximum).

We also used the temperature minimum in order to determine water column overturning during the previous winters following the reasoning of Rudels et al., (1996). These calculations require more consideration due to peculiarities of the regional water mass distribution and are properly discussed in the next section together with the large-scale hydrography.

A "mixed layer" depth is often used by oceanographers to describe vertical scales in the surface layer. This well-mixed layer is in contact with the atmosphere and separated from deeper waters by a sharp density gradient (Schmidtko et al., 2013; Peralta-Ferriz and Woodgate, 2015). Even beyond the caveat that being "well-mixed" does not necessarily imply "actively mixing" (Brainerd and Gregg, 1995), density profiles in the rapidly melting MIZ often do neither exhibit a well-mixed surface layer nor a clear density step below, making it impossible to relate either to the turbulence (Morison et al., 1987; Randelhoff et al., 2017; Dewey et al., 2017) because such a traditional "mixed layer" depth is often $\ll 10$ m (Figure S2.1).

Instead, we make reference to the "equivalent mixed layer depth" h_{BD}, a metric previously developed by Randelhoff et al. (2017) for strongly meltwater-influenced surface waters in the MIZ. Equivalent mixed layer depth is defined as $h_{BD} = BD/\Delta\sigma_\theta$, where BD is the vertically integrated buoyancy deficit compared to a reference state, taken to be the shallowest depth that is not affected by seasonal density variations, and $\Delta\sigma_\theta$ is the difference between densities at that reference depth and the surface, usually an average over the upper meters. Those authors found that the equivalent mixed layer depth h_{BD} constrained the extent of vertical mixing well. The same will be shown to hold for the present data set which also includes vertical profiles of turbulent mixing.

Turbulence and vertical mixing

Turbulent microstructure in the upper 100 m was sampled at stations selected to represent the entire spectrum of ice and stratification conditions using a "Self-Contained Autonomous MicroProfiler" (SCAMP, Precision Measurement Engineering, California, USA). The SCAMP was deployed from a small craft approximately 1 nautical mile from the vessel to avoid noise contamination, free falling at approximately 10 cm s^{-1} and with up to 5–6 repeat casts at each station.

The dissipation rate of turbulent kinetic energy ε was obtained from fitting the theoretical Batchelor spectrum to the temperature gradient microstructure spectrum using the modified maximum likelihood method of Ruddick et al. (2000). More details concerning the method

can be found in Cuypers et al. (2012). The diapycnal diffusivity K_z was parameterized using Osborn's formulation (Osborn, 1980). It has been argued that a constant mixing efficiency $\Gamma = 0.2$ may overestimate the vertical diffusivity at high turbulence intensities, e.g. at weak stratification (Shih et al., 2005; Bouffard and Boegman, 2013). For typical ranges of oceanic turbulence, $\Gamma = 0.2$ fits in situ data and agrees with proposed alternative parameterizations (e.g., Bouffard and Boegman, 2013, in particular their Figure 8c), and so we chose $\Gamma = 0.2$ for consistency with results reported earlier (Gregg et al., 2018).

In keeping with Brainerd and Gregg (1995), we defined a mixing layer depth h_ε as the depth where ε drops below $5 \cdot 10^{-9}$ W kg^{-1}, which is well below values observed in the surface layer, but larger than the background dissipation rate measured below the pycnocline, both in their study and in our data.

Inorganic nutrients

Water samples were collected at each hydrographic station for determination of inorganic nutrients (nitrate NO_3^-, nitrite NO_2^-, phosphate PO_4^{3-}, and silicic acid $Si(OH)_4$). Samples from Niskin bottles on the CTD rosette were pre-filtered through a GF/F filter and stored in acid-washed and sample-rinsed 15-ml polyethylene tubes. These samples were then either stored at most a few hours at 4°C in the dark or analyzed immediately on a Bran+Luebbe Autoanalyzer 3 using standard colorimetric methods (Grasshoff et al., 1999). Analytical detection limits are: 0.02 μmol l^{-1} for NO_2^-, 0.03 μmol l^{-1} for NO_3^-, 0.05 μmol l^{-1} for PO_4^{3-} and 0.1 μmol l^{-1} for Si.

We derived a "nitracline depth" as the shallowest depth where NO_3^- concentration exceeded 1μM, based on a linear interpolation from the 10 m vertical resolution in the relevant depth range to a vertical spacing of 1 m.

We refined the discussion of the water masses beyond their temperature-salinity properties by additionally taking their phosphate and nitrate signatures into account. Following Newton et al. (2013), we calculated the "Arctic N-P relationship" (ANP). Essentially, ANP = 0 means the $NO_3^- - PO_4^{3-}$ pairs fall on the regression line for Atlantic Water, whereas for ANP = 1 they fall on the regression line for Pacific-derived water. In this study, we used the N-P regression lines by Jones et al. (1998) which according to Tremblay et al. (2015, their Figure 1) also hold in northwestern Baffin Bay, the source of the waters observed in the western ends of the Green Edge transects.

Clustering stations into Arctic and Atlantic water

To subsume and visualize the pervasive east–west gradient of hydrographic variables that will be apparent across the station grid, and circumvent the limitations of water masses that are traditionally only defined in terms of salinity and temperature, we used a fuzzy c-means clustering algorithm (Section S5) to cluster hydrographic variables, including nutrient tracers, into two lateral domains: Arctic and Atlantic.

The following properties were included to define two clusters, centered and normalized: (1) maximum temperature in the AW layer, (2) salinity at the estimated convection depth, and (3) ANP at 20-m depth. These properties

summarize the strength of Atlantic inflow and the resulting hydrography and nutrient composition.

Wind velocities

We used the CCMP V2.0 wind vector analysis product (Atlas et al., 2011), downloaded from http://www.remss.com/measurements/ccmp, to extract the 10-m surface wind field for our study area.

Sea ice cover

We defined the ice edge as the contour line where the ice concentration c was 15%, as given by AMSR2 sea ice concentration data on the 3.125-km grid (Spreen et al., 2008), downloaded from http://www.iup.uni-bremen.de:8084/amsr2data/asi_daygrid_swath/n3125/.

For each hydrographic station, we calculated an "open water days" (OWD) parameter based on how long it had been ice-free or how long it took to become ice-free, as quantified by the days of $c < 15\%$ since day of year (doy) 120 (April 29) or the days with $c > 15\%$ until doy 210 (July 28), respectively. For more detail, see the supplemental material.

Light

A photosynthetically available radiation (PAR; mol photons m^{-2} d^{-1}) level of 0.415 mol m^{-2} d^{-1} has been found to bound the lower extent of the vertical phytoplankton distribution in the North Pacific subtropical gyre (Letelier et al., 2004) and has been used in the North Atlantic for the same purpose (Boss and Behrenfeld, 2010). To assess the underwater light climate, we computed the depth of this isolume by combining 1) 40 profiles of multispectral underwater irradiance using a "Compact Optical Profiling System" (C-OPS, Biospherical Instruments, Inc.) and 2) a composite dataset of daily above-surface irradiance, PAR^{0+}.

Lacour et al. (2017) derived a lower value of 0.1 mol m^{-2} d^{-1} for the lower extent of possible phytoplankton growth for the subpolar North Atlantic. Qualitatively, the two criteria agree, with isolumes at the 0.1 consistently around 15 m deeper than at the 0.415-mol m^{-2} d^{-1} level (Figure S4.3). However, choosing such an isolume level is somewhat arbitrary when applied in the field, being the mean over a set of different species in different conditions, not representing hard limits for any given species as they would for laboratory studies Geider et al., 1986). For this study, we chose the 0.415-mol m^{-2} d^{-1} threshold, firstly because it is the value commonly applied at lower latitudes and hence less subjective, and because it is a conservative value. Hence, in the following, "isolume" always refers to the 0.415 mol m^{-2} d^{-1}-level, unless explicitly stated.

Letelier et al. (2004) originally measured scalar irradiance (E_o) using a spherical sensor, whereas the C-OPS used in this study measures planar irradiance (E_d). Modelling by Pavlov et al. (2017, their Figure 9) in and around an under-ice phytoplankton bloom indicates that the ratio $E_o : E_d$ is within the range of 1.3–1.6, meaning that by using E_d, we underestimate the depth of any isolume by a factor of at most approximately log $(E_o/E_d)/K_d$ (PAR) $\approx$ 1–7 m, where K_d (PAR) $\approx$ 0.07–0.25 m^{-1} is the diffuse attenuation coefficient of PAR as observed in our dataset. Again, this analysis serves to show that the isolume depths discussed in this paper are conservative.

Additional caveats include that the light field under a heterogeneous cover of ponded ice floes and leads between them is notoriously difficult to parameterize (Massicotte et al., 2018), with spatial heterogeneity of the ice cover Frey et al., 2011; katlein et al., 2015) and horizontal spreading of light under the ice (Ehn et al., 2011) being major issues. Nor is it clear whether the physiological response of the phytoplankton is governed by the daily average light field or by sub-daily variations, e.g., through exploitation of or disruption by peak irradiance in leads.

In summary, the isolume depths computed in this paper should be seen as indicative of the depth range where growth definitely was possible, rather than the physiological maximum.

Incoming above-surface irradiance

PAR just above the sea surface was estimated using both (1) in situ data recorded on the ship meteorological tower (Kipp & Zonen PAR Lite; sampling frequency 1 min^{-1}) and (2) an atmospheric radiative transfer model (SBDART, Ricchiazzi et al., 1998). SBDART was first validated against in situ measurements (Figure S4.5), and then used to derive 24-hour mean irradiance at a given location before the hydrographic station. SBDART yields more reliable results for these daily irradiances because the in situ measurements were likely strongly affected by changing ice albedo and fog conditions as the CCGS *Amundsen* traversed back and forth across the MIZ.

SBDART was implemented using precomputed lookup tables as described by Laliberté et al. (2016). Briefly, spectral downwelling irradiance at wavelengths of 290–700 nm (5-nm intervals) was estimated with 1-hour resolution as a function of solar zenith angle, surface albedo, cloud optical thickness (COT), total ozone column (O$_3$), and cloud fraction (CF). COT, O$_3$ and CF were obtained from MODIS atmosphere (https://modis-atmosphere.gsfc.nasa.gov/) Collection 6. Surface albedo was estimated from sea ice concentration as retrieved by the AMSR2 microwave satellite sensor (see above) based on Perovich and Polashenski (2012).

Underwater irradiance

The C-OPS was deployed either from small craft, or through a hole in the ice when it was thick enough to permit working on it. Vertical profiles of downwelling irradiance were measured down to 100 m depth. Concurrently, above-surface downwelling irradiance (PAR^{0+}) was measured using another sensor which serves as a reference to calculate the transmittance of PAR in the water column as the ratio between the in- and the above-water measurements (also called the PAR percentage below). More details can be found in the supplemental material.

Multiplying daily above-surface irradiance PAR^{0+} by the PAR percentage gives a vertical profile of the daily PAR. In order to correct for variable sea ice concentration (and the fact that not all ice-covered stations could be sampled from the sea ice), a composite under-ice (under-water) profile was constructed using the closest available measurement of ice (water surface) transmittance (**Figure 3B**) for each station sampled from open water (ice, respectively). Weighting the water and ice profiles according to
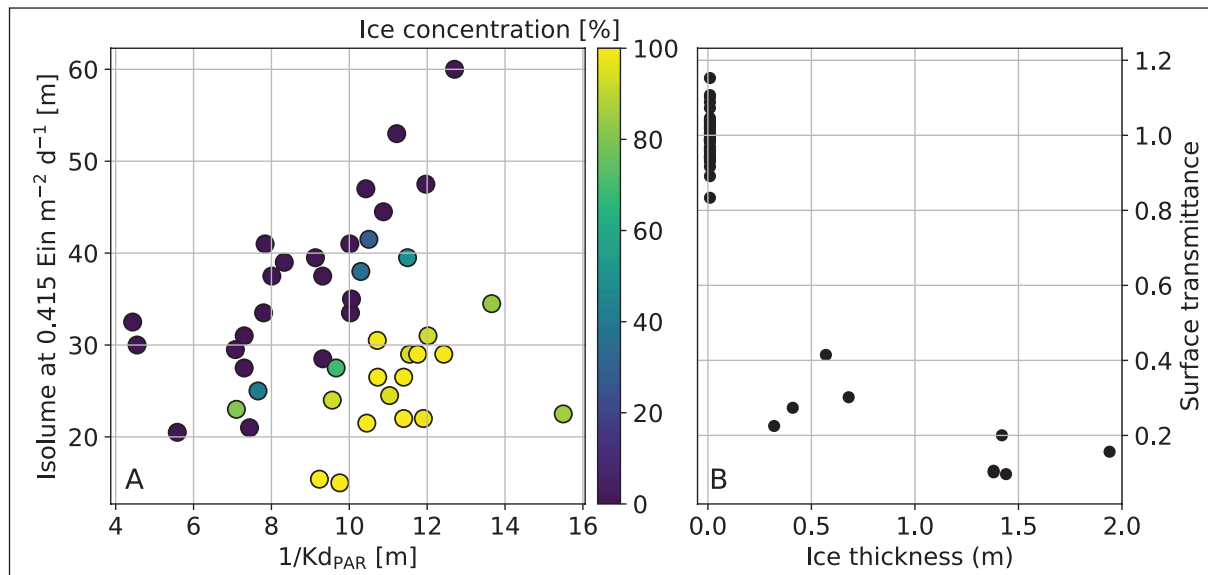
Figure 3: The underwater light field. A: The depth of the 0.415 mol m^{-2} d^{-1} isolume as a function of water-column PAR attenuation e-folding scale (1/K$_d$); ice concentration inferred from AMSR2 as color shading. **B:** Ratio between shallowest measured in-water PAR as seen by the C-OPS, and surface PAR. For ice thicknesses larger than 0 m, this is an approximation of the combined ice+snow transmittance; see Figure S4.2 for a map. DOI: https://doi.org/10.1525/elementa.357.f3

the AMSR2-derived sea ice concentration, we calculated a vertical PAR profile, to which the 0.415 mol m^{-2} d^{-1} criterion was applied to derive the isolume depth.

Chlorophyll-a

For detection of the chl-a maximum concentration along the vertical profile, we used output from the rosette-mounted Seapoint Fluorometer. CTD processing includes the manufacturer calibration against biomass in laboratory cultures, but was not corrected for in situ fluorescence-biomass relationships. Because of the possibility of quenching during daytime, we also assessed beam attenuation as measured by a transmissometer as a proxy for biomass and derived the depth of its maximum value for each profile.

For more detailed comparison with phytoplankton biomass, we used total chlorophyll-a (TChl-a) concentrations calculated from photosynthetic pigment measurements at a total of 41 stations. The analytical procedure is described by Ras et al. (2008). Briefly filters were extracted for two hours in 100% methanol, disrupted by sonication and clarified by filtration (GF/F Whatman, then 0.2 m polytetrafluoroethylene filter). The samples were analyzed using high-performance liquid chromatography (HPLC) the same day, using an Agilent Technologies HPLC 1200. A C8 guard column was installed before the analytical column.

Results and Discussion, part 1: The large-scale hydrography of southern Baffin Bay
Ice edge retreat

Until approximately doy 160, the ice edge lingered over the West Greenland shelf break and extended onto the shelf. Around doy 165, retreat started from the north and by doy 190, one month later, the ice edge was rapidly approaching the Baffin Island shelf break (**Figure 2A**). The ice edge moved on average 9 km from day to day, but

the overall net westward displacement was somewhat slower at 3.5 km d^{-1} (**Figure 4A**).

We also used OWD, just like the spatial distance from the ice edge, to position hydrographic stations relative to the ice cover; the two quantities were well correlated (**Figure 5**) with a slope of 4 km d^{-1}, reasonably close to the net westward displacement, and even better so when local variations were taken into account (ice edge retreat covered a larger distance further north).

The interior ice pack away from the ice edge was rather compact with concentrations upwards of 95% in most places (**Figure 2B–D**), up until around doy 190 (July 8), when the Green Edge campaign ended. After that, the ice cover deteriorated quickly from doy 195 with ice concentrations dropping below 75% in most places even hundreds of kilometers beyond the ice edge (**Figure 2E**); the entire study grid was ice-free by doy 210 (July 28; not shown). Specific events such as the rather large fluctuation of the ice-edge position between doys 165–170 (**Figure 4B**) may have influenced the overall deterioration of the ice cover, but there is little evidence that general patterns in wind or incident solar radiation (**Figure 4C**) drove ice retreat and melt. In particular, the retreat averaged over the study area seemed to be mostly due to ice melt because there were no persistent easterlies during the cruise that could have pushed the ice west.
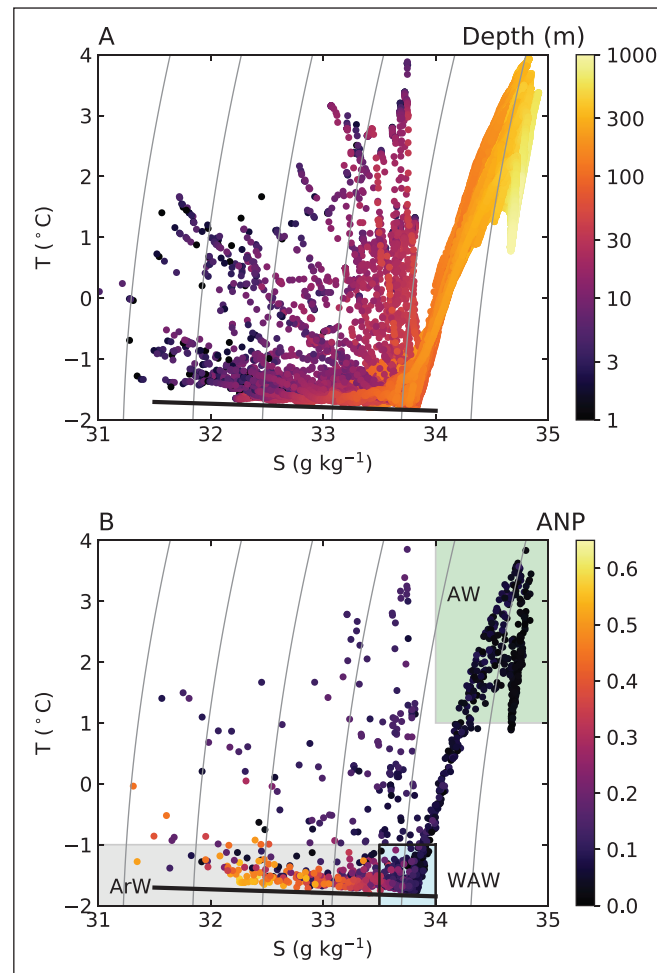
Water masses

Temperature-salinity plots (**Figure 6**) showed the presence of warm Atlantic-derived water to the east of the station grid (**Figure 7**), a bend at salinities just below 34 g kg^{-1}, and a "cold halocline"-like layer extending to the surface. Warmed surface water was also present at very variable temperatures and salinities; it was mostly located in the eastern half where the ice had retreated earliest.
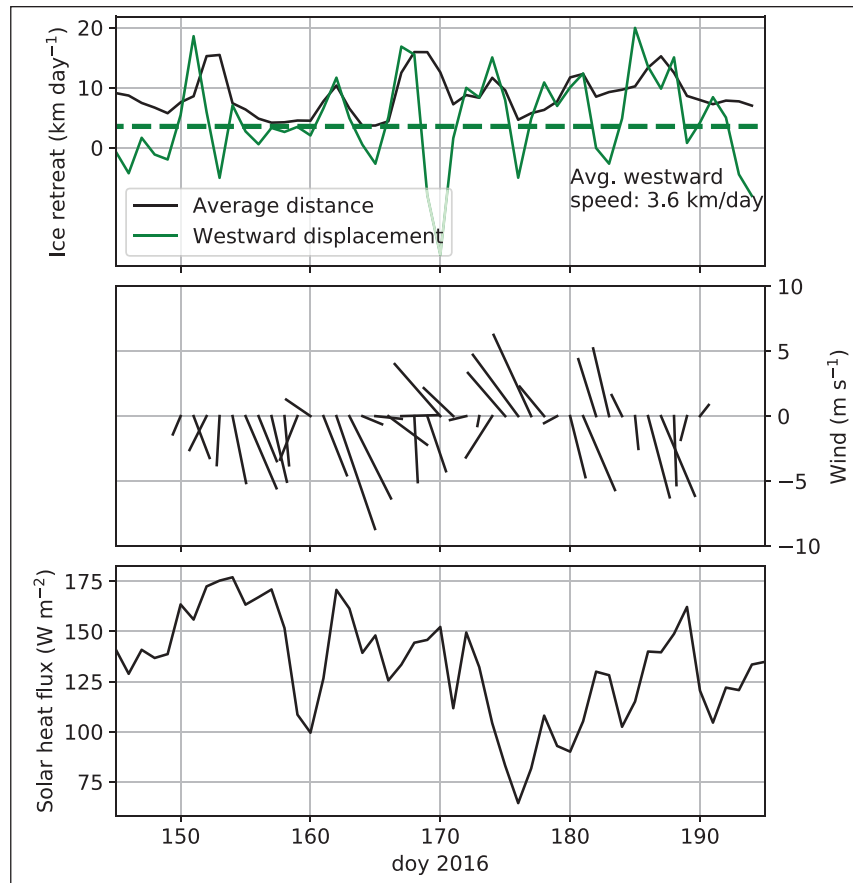
Figure 4: Dynamics of the ice edge retreat. A: Ice retreat speed. Mean distance between ice edges on consecutive days (black); day-to-day displacement of average ice-edge position westward (green), i.e., positive numbers are westward, negative eastward. **B:** Wind vectors averaged over the study area. **C:** Daily incoming surface irradiance averaged over the study area. DOI: https://doi.org/10.1525/elementa.357.f4
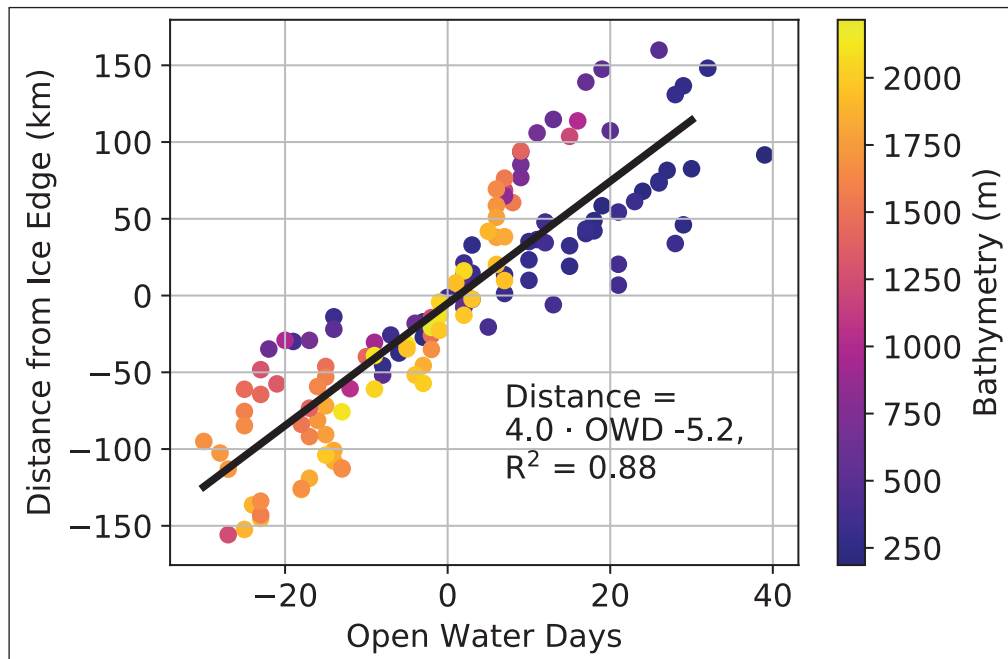
Figure 5: Distance from the ice edge as a function of open water days. The color scale indicates bottom depth, thus implicitly hydrographic regime, and shows that an even better one-to-one correspondence is reached when considering geographical subsets of the relation. The slope of the regression is another way of examining the ice edge retreat speed, which can also be inferred from the average westward displacement of the ice edge, see Figure 4A. DOI: https://doi.org/10.1525/elementa.357.f5

Figure 6: Water masses as determined from salinity, temperature, and nutrient concentrations. T-S plots with absolute salinity and conservative temperature; σ_θ isolines in gray, freezing point relation at 0 dbar as thick, black line. **A:** Color scale indicates water depth of measurement. **B:** The shaded areas represent water mass definitions; ArW: Arctic Water, AW: Atlantic Water, WAW: Winter Atlantic Water. The color scale indicates ANP following Newton et al. (2013). DOI: https://doi.org/10.1525/elementa.357.f6

The studies by Tang et al. (2004) and Zweng and Münchow (2006) represent the most recent large efforts to synthesize data on Baffin Bay hydrography; the former is ambiguous, however, on the exact definitions of the water masses, giving a qualitative rather than quantitative picture (see their Figure 14). The latter is more explicit, but still lacks tracers other than temperature and salinity. We have chosen to modify and align their definitions, but retain the general water masses (though Baffin Bay Deep Water at depths below 800 m is not treated here). Our definitions are as follows.

(1) An Atlantic-derived water mass with $T_C > 1°C$ and $S_A > 34.0$ g kg^{-1}, from here on called *Atlantic Water* (AW). In the literature, this has also been called, inter alia, "West Greenland Intermediate Water", "Baffin Bay Intermediate", "Atlantic Intermediate", and "Arctic Intermediate" (according to Tang et al. (2004)). Such nuances are not needed here as the study area is well-confined; hence we chose the simplest term. In addition, the N-P relation in this water mass is within ANP ≤ 0.1 of the one derived by Jones et al.(1998) for AW.

(2) *Arctic Water* (ArW) with $T_C < -1°C$ and $S_A < 33.5$ g kg^{-1}. In this water, we observed an N-P signature of ANP ≥ 0.2 but well within 0.6. Note that the Pacific nutrient signature of Jones et al. (1998), while fully present in northwestern Baffin Bay (Tremblay et al., 2015), is strongly diluted by Atlantic Water, in a ratio of approximately 1:1, in the Green Edge area. Comprised in this ArW is a layer similar to the *Cold Halocline Layer* (CHL) of the Arctic Ocean proper, a salinity-stratified but homogeneously cold layer of water.

(3) *Winter Atlantic Water* (WAW) with $T_C < -1°C$ and 33.5 g kg^{-1} < S_A < 34.0 g kg^{-1}, which represents the temperature-minimum bend in the T-S diagrams that occurred in most profiles apart from the ones sampled closest to the Arctic current. Notably, this water mass was not present in the observations made at the ice camp (Oziel et al., 2019), meaning it likely originated from the Atlantic rather than the Arctic sector (see next section on convection).

ANP showed a clear east–west gradient that reflects the differences between the two main water masses (**Figure 6B**).
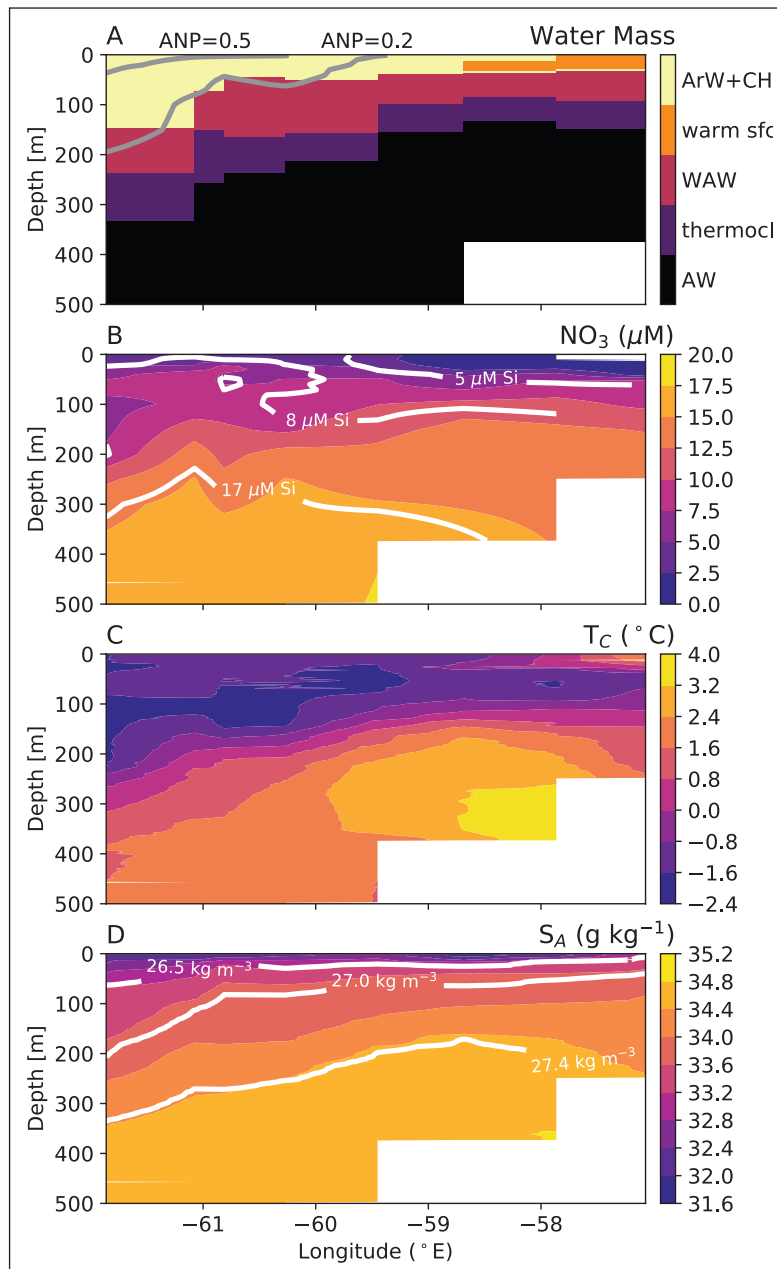
Figure 7: Hydrographic section along 68°N. A: Water masses as defined in the text; **B:** Nitrate concentration as color shading, silicate as isolines; **C:** Temperature; **D:** Salinity as color shading, potential density as isopycnals. This transect is representative for all seven transects discussed in this study. DOI: https://doi.org/10.1525/elementa.357.f7

The highest ANP value observed in the *Amundsen* station grid in 2016 was just short of 0.7, with more usual values typically around 0.5 inside the core of what we have defined as the Arctic Water mass (ArW). These values indicate a 50–50% dilution of the Pacific Water coming from northwestern Baffin Bay, reflecting a strong inflow of Atlantic Water in this area. However, the 2016 CCGS *Amundsen* station grid probably did not capture the core of the southward current, most of which we would expect to be over the Baffin Island shelf slope. In fact, at the ice camp, just next to the coast, ANP values in excess of 0.8 were sometimes observed in the upper 60 m (Oziel et al., 2019), an overwhelming Pacific signature. However, the mean of the entire 2016 ice camp period was similar if somewhat higher (0.6) to that of the closest station in the CCGS *Amundsen* station grid (**Figure 8E**).

Convection and the pre-bloom nutrient inventory
Water that results from wintertime cooling and possibly brine rejection is close to the freezing point, whereas the Atlantic Water below is warmer, as is the surface water warmed by solar radiation in summer. Identifying the temperature minimum in a relevant depth range helps to locate the overturning depth of the previous winter (Rudels et al., 1996). However, strictly speaking, this minimum represents a water mass that at some point must have been ventilated during winter; it thus represents an upper bound on the overturning depth only. In the following, we distinguish between the absolute temperature minimum of a CTD profile as a water-mass marker, and local temperature minima as indicators of recent winter overturning.
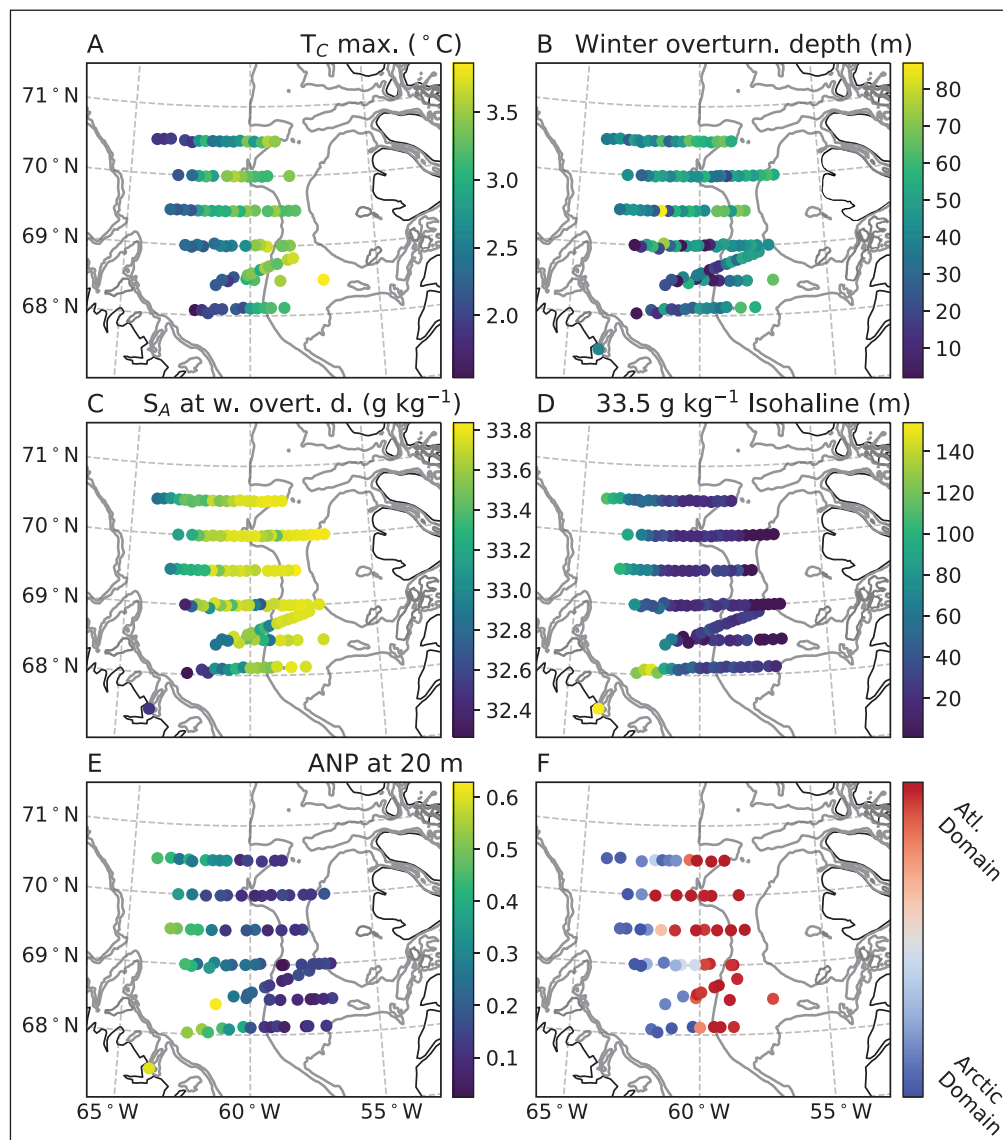
Figure 8: Key hydrographic properties across the station grid. A: Maximum AW temperature, a proxy for inflow from the south. **B:** Depth of the estimated winter overturning depth. **C:** Salinity at this estimated overturning depth. **D:** Depth of the 33.5 g kg⁻¹ isohaline, the lower extent of what is classified as ArW. **E:** The ANP tracer (see text) at 20-m depth. **F:** Classification of the Atlantic and Arctic Domains, based on fuzzy clustering of maximum temperature in the AW layer, ANP at 20-m depth, and salinity at the estimated convection depth (see text). Selected cluster-averaged values are listed in Table 1. Where applicable, the corresponding values sampled at the 2016 ice camp are shown for reference (Oziel et al., 2019). In grey: Isobaths at 250 and 500 m. Similar figures for other parameters are shown in the supplemental material, see Figures S2.1 to S2.10. DOI: https://doi.org/10.1525/elementa.357.f8

Winter Atlantic water and the temperature minimum

In the western part of the station grid, absolute temperature minima ranged between 100 and 150 m, consistent with Tang et al. (2004). However, it is unlikely that these depths actually represent local convection. For instance, one notes that the sharp bend at salinities of 33.5–34.0 g kg⁻¹ is eroded in the western transects (**Figure 6A**) and in particular at the ice camp (Oziel et al., 2019). Also, ANP values (the Pacific contribution to these waters) at the depth of the absolute temperature minimum are usually close to 0 (**Figure 6B**). Both of these facts indicate that the source of these occasionally occurring intrusions of minimal temperature lies in the eastern parts of the Basin; we hypothesize that the intermediate water at 33.5–34.0 g kg⁻¹ represents the remnant of previously convecting Atlantic-derived

water that was subsequently subducted under ArW and isolated from convection (and hence we called it WAW, Winter Atlantic Water), rather similar to the formation mechanism of the Lower Cold Halocline in the Arctic Ocean proper as proposed by (Rudels et al. (1996); see also Woodgate et al. (2005). Our data set does not permit further corroboration of this hypothesis; more detailed investigation awaits future studies, likely involving other chemical tracers.

Winter mixed layer depths, convection, and local temperature minima

To find a recent overturning depth and with it the pre-bloom surface nutrient concentration, more care is required. Many of the temperature profiles exhibit local extrema, meaning that the shallowest of the local minima likely represents

recent convection or winter mixing. One may have reservations about this method in the case of very shallow (to a few tens of meters) temperature minima, given the fast dynamics of the surface layer that may distort temperature profiles between winter and summer. However, this reasoning is the best approximation that is available to us using data only sampled during summer and should ultimately be replaced by wintertime measurements.

We chose the shallowest local minimum (over a window of 20 m) of freezing point deviation not exceeding 0.3°C, but the conclusions are not sensitive to the exact threshold; however, these criteria were chosen after visual inspection of the collected profiles and do not represent a globally valid method (Figures S6.1 and S6.2).

Estimated winter mixing layer depths ranged between 10 and 90 m, or salinities of 32.3 to 33.8 g kg^{-1}, the shallowest and freshest of these being closest to the Baffin Island shelf (**Figure 8B, C**), which is consistent with the hydrographic profiles sampled at the ice camp itself (Oziel et al., 2019). The sometimes large variability between neighboring stations reflects to some extent the arbitrariness in selecting the overturning depth, but also the hydrographic variability with frequent interleaving of water masses evident in the CTD profiles (Figure S6.2). Here we are interested in the regional averages of the overturning depth, not the overturning depth at particular stations.

Arctic and Atlantic domains in Baffin Bay

The overwhelming majority of hydrographic variables showed a clear east–west gradient, such as the maximum temperature, its depth, the depth of the 33.5 g kg^{-1} isohaline, and nutrient concentrations (**Figure 8**). The fuzzy clustering (see Methods) reproduced as expected the longitudinal gradient present in virtually all variables (**Figure 8F**). Estimated convection depths for Arctic and Atlantic domains lie around the 33.0 and 33.7 g kg^{-1} isohalines, respectively (**Table 1**). The estimated salinity at the base of the winter mixed layer in the Arctic domain (33.0 g kg^{-1}) falls around halfway between the Atlantic domain and $\approx$32.5 g kg^{-1}, which was observed both at the 2016 ice camp and the southwestern extreme of the *Amundsen* sampling grid.

Table 1: Physical and biogeochemical characteristics of the Arctic and Atlantic domains. Domains determined by the clustering as described in the text (see also Figure 8; thresholds for the membership function <0.1 and >0.9, respectively). DOI: https://doi.org/10.1525/elementa.357.t1

Parameter	Arctic	Atlantic
T_C max. (°C)	2.1	3.3
Depth of winter overturning (m)	34	50
NO_3^- at winter overturning depth (μM)	6.5	8*
S_A at winter overturning depth (g kg^{-1})	33.0	33.7
Ice concentration (%)	75	35
Depth of S_A 33.5 g kg^{-1} isohaline (m)	81	24

* Likely reduced by nitracline deepening (see text).

While nitrate consumption in the western part had not generally reached that overturning depth (nitrate uptake had just started at the surface; see **Figure 7**), most profiles sampled in the eastern part exhibited a well-delineated deep chl-a maximum (**Figure 9E**). In particular, in the Atlantic sector, the winter overturning depth was located well inside the WAW and thus likely tapped into the Atlantic nutrient pool of relatively high nitrate (around 10 μM), while for the Arctic domain, a more likely pre-bloom nitrate concentration was 6 μM (Figure S2.15). At the ice camp, maximum winter concentrations of NO_3^- were 4–5 μM (Oziel et al., 2019), consistent with the lower surface concentrations observed in the southwesternmost part of the station grid.

What we call here "Arctic" and "Atlantic" is to be understood only relative to the context of the Green Edge CCGS *Amundsen* data set — the clustering includes no external information about what constitutes either of those categories, even though it reproduces them well. In particular, the southwesternmost stations (located closest to the ice camp) are much more similar to the ice camp in terms of hydrographic variables than most of what we have classified as the Arctic domain (Oziel et al., 2019). This similarity is a matter of the point of reference; most of the CCGS *Amundsen* station grid presented in this article did not capture the core of the southward flowing current of Arctic water.

Results and Discussion, part 2: Surface layer dynamics and light climate

Upper ocean dynamics in the context of the large-scale hydrography

Water column stratification differed markedly between the Arctic and Atlantic (or, western and eastern) domains that we delineated above, which reproduced the overall pattern between different areas of the Arctic Ocean. On one hand, those areas dominated by the weakly thermally stratified inflow of Atlantic Water, where winter convection often reaches far into the deeper nutrient-rich waters and leads to high upward nutrient fluxes (e.g., Carmack, 2007; Randelhoff et al., 2015).

On the other hand, other areas feature a strong haline stratification, such that not even wintertime brine rejection leads to overturning beyond the photic zone. This is the case in the strongly Pacific-influenced Chukchi and southern Beaufort seas, where density mixed layers only reach 20–40 m in depth (Peralta-Ferriz and Woodgate, 2015). We observed similar depths in the southwestern end of the Green Edge station grid (**Figure 8B**), where strongly stratified Arctic water capped the upper 40–50 m. At the ice camp, winter overturning reached to around 40-m depth, but the corresponding salinities and thus nutrient concentrations agreed well between the ice camp and the closest CCGS *Amundsen* stations (**Figure 8B, C**; Oziel et al., 2019).

Winter overturning (or the lack thereof) determines the inorganic nutrient pool and stratification for the next spring. The following section focuses on the upper ocean dynamics, mostly forced by gradients in the ice cover. The longitudinal gradient in the ice cover, however, will be partially confounded with the overall regional (non-seasonal)
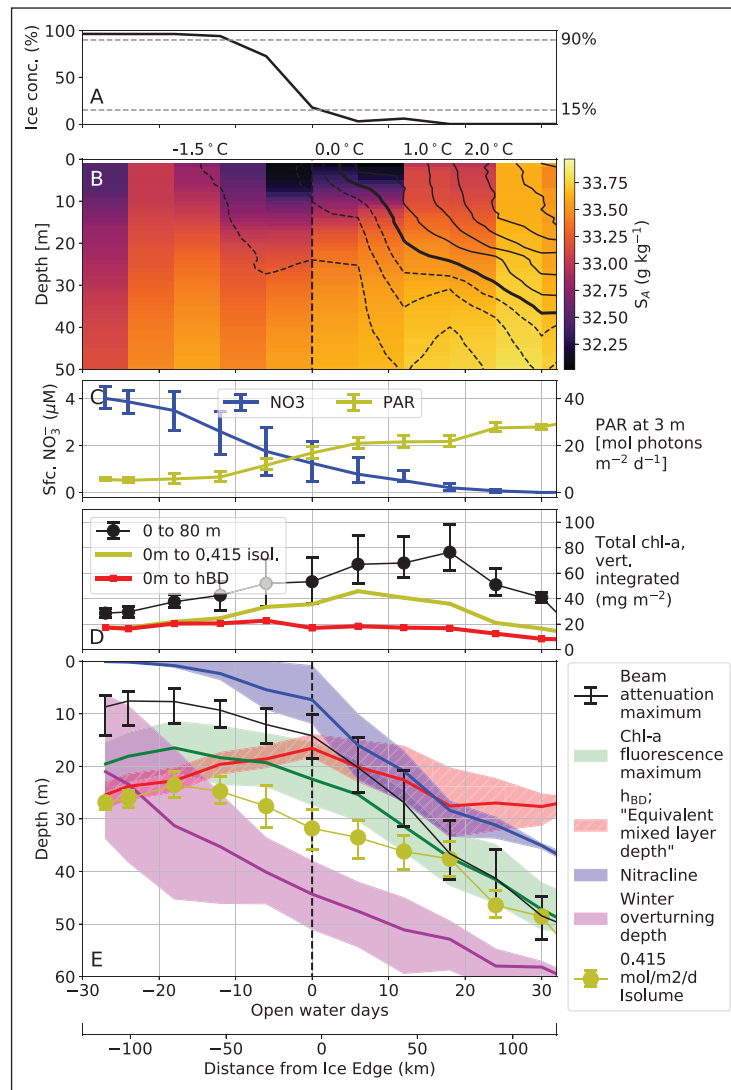
Figure 9: Composite cross ice edge transect. An average of all transects binned by OWD (the "open water days"
variable). The "distance from the ice edge" axis is re-calculated from the regression in Figure 5. **A:** Ice concentration.
B: The color scale shows salinity, the contour lines temperature as indicated on the top of the panel. **C:** Surface nitrate
concentration and PAR irradiance at 3 m depth. **D:** Phytoplankton standing stock integrated from the surface to the
isolume (grey line) and from the surface to 80 m depth (green line). **E:** Vertical layers of interest: The nitracline; the
extent of the surface layer, h_{BD}, which places a limit on the extent of the mixing layer; the chl-a fluorescence maxi-
mum depth; the depth of maximum beam attenuation, a proxy for biomass, and the depth of the 0.415 mol m^{-2} d^{-1}
isolume. The estimated depth of winter overturning is shown for reference. Shaded areas and error bars show 25 and
75% quantiles. DOI: https://doi.org/10.1525/elementa.357.f9

water mass dynamics in the west where winter overturn-
ing does not reach deeper than the typical extent of the
summertime meltwater-stratified ice-ocean boundary
layer of around 40-m depth (Randelhoff et al., 2017).

Vertical scales in the surface layer

Irradiance and isolume depth
Isolume depths defined at the 0.415 mol m^{-2} d^{-1} level
displayed a large range from 15 to 55 m. This variability
was caused almost completely by variations in attenua-
tion of incident surface PAR (sea ice concentration and
K_d) rather than variations in surface irradiance, as is
evidenced by a tight correspondence between isolume
depth and euphotic zone depth Z_{eu} (**Figures 3A**, S4.1);
in fact, the 0.415 mol m^{-2} d^{-1} isolume depth and
the

euphotic zone depth were not significantly different. Z_{eu}
was defined as the depth to which 1% of surface irradi-
ance was transmitted, based on the observed underwater
irradiance (C-OPS) profiles. Whereas the clearest waters
($1/K_d = 13$ m) at open water sampling sites had isolume
depths in excess of 50 m, a shoaling to around 20 m was
observed by either a 50% reduction in $1/K_d$, or going
from 0 to 100% ice cover.

Combined ice+snow transmittance was for the most
part <0.3 (**Figure 3B**) and smallest (0.05–0.2) for the
thickest ice (Figure S4.2). However, transmittances were
evidently large enough that even at ice concentrations
close to 100%, isolumes between 15 and 30 m were
observed (**Figure 3A**), covering most of the surface layer
defined by h_{BD}.

A composite cross-ice-edge transect

Because the summer ice edge retreat in Baffin Bay was so steady, the usual problem of confounding time and space variability was tractable in our dataset. In essence, open water days (OWD) and the distance from the ice edge were well correlated. Having binned and averaged all hydrographic stations according to their OWD value, we can consider representative cross-ice-edge transects.

Freshening by ice meltwater was most pronounced in a ±15 day (or ±60 km) window around the ice edge (**Figure 9**). A slight warming of the surface ocean started already at a similar distance into the ice, but picked up rapidly only once low ice concentrations of around 15% were reached. The equivalent mixed layer depth, h_{BD}, first shoaled from about 25 m at OWD≪0 to 15 m at OWD = 0 days, and deepened again once the ice had disappeared. This pattern reproduced the findings of Randelhoff et al. (2017) for the Barents Sea MIZ.

Surface nitrate concentrations decreased simultaneously (**Figure 9C**), and the surface layer was already NO_3^--depleted in parts as early as OWD≈ −15 days, as evidenced by the fact that the average nitracline was no longer at the surface. Whether this consumption was due to ice algae or phytoplankton is not clear, but the latter seems more likely in view of the timing of the ice-algal and pelagic bloom at the ice camp (Oziel et al., 2019), and the presence of a standing stock of phytoplankton. Only after considerable nitrate depletion in the surface layer did the subsurface chl-a maximum deepen (starting from about from OWD = 0 days). Although a subsurface maximum of chl-a fluorescence appeared throughout the time series, for OWD < −10 days it was very weak, likely representing mostly photoacclimation (more chl-a per biomass in deeper cells) or daytime chlorophyll quenching instead of a subsurface biomass maximum, as indicated by the fact that the beam attenuation maximum was only half as deep during that time.

The strong surface stratification, implied by shallow equivalent mixed layer depths h_{BD}, also inhibited mixing (**Figure 10**) and consequently upward fluxes of nutrients (Randelhoff et al., 2016). However, only when the nitracline deepened below the surface layer defined by h_{BD}, and consequently decoupled from most of the wind-driven mixing (Randelhoff et al., 2017), was the surface layer productivity restricted by the upward turbulent flux of nitrate. The chl-a maximum responded to this nutrient depletion by staying
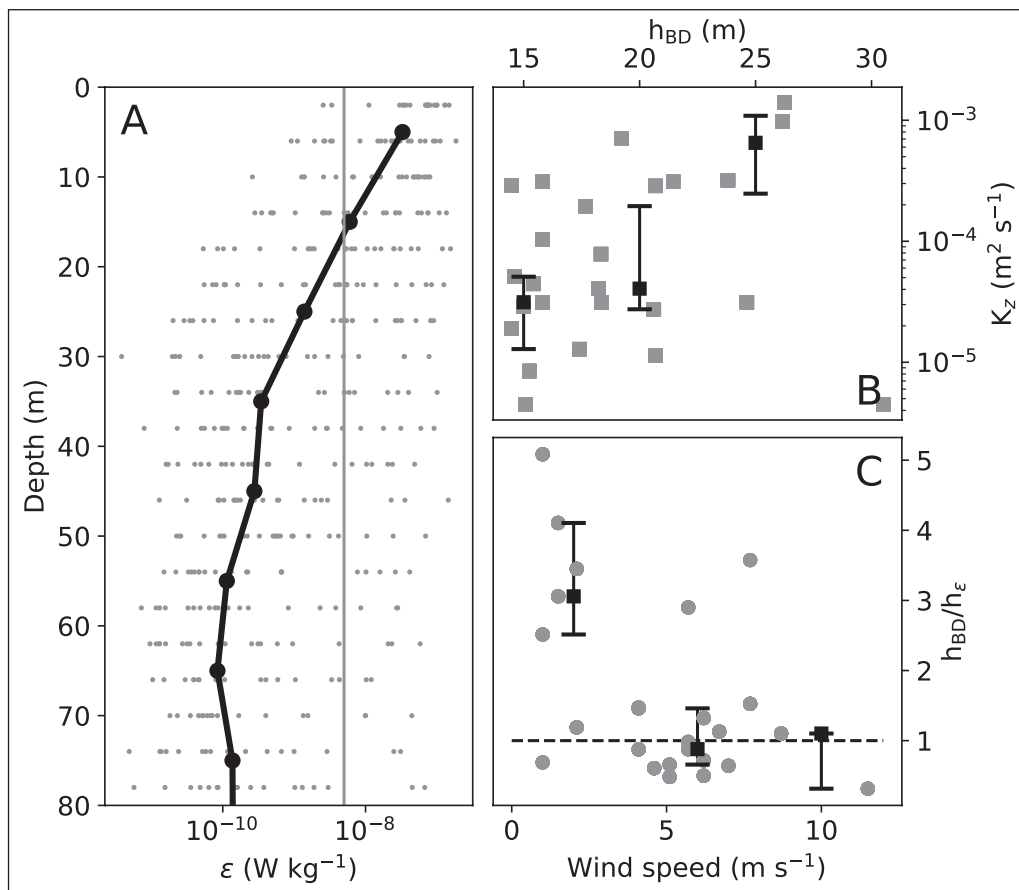
Figure 10: Turbulent mixing observed in the surface ocean. A: Dissipation rate of turbulent kinetic energy (ε) over the upper water column. Black line: Median dissipation profile. Note that this median represents the "most often occuring" profile, not the *mean* dissipation; the latter is hard to compute as dissipation values are likely sampled from different distributions (owing to different environmental forcing) for different profiles. Vertical grey line: 5.10^{-9} W kg^{-1} cutoff for the computation of the mixing layer depth h_ε. **B:** 5–25 m averaged K_z as a function of h_{BD} (equivalent mixed layer depth). **C:** Ratio of h_{BD} to mixing layer depth h_ε as a function of wind speed. In panels B and C, the black squares and error bars indicate bin-wise 25, 50, and 75% percentiles. DOI: https://doi.org/10.1525/elementa.357.f10

below the nitracline (see also Figure S6.5). The nitracline, h_{BD}, isolume, and chl-a maximum were all in the 20–40 m depth range at approximately OWD = 10 days. Later, at OWD≫10 days, the deep chl-a maximum was perched between the nitracline and the 0.415 mol m^{-2} d^{-1} isolume: phytoplankton likely accumulated where the compromise between availability of nutrients and sunlight was optimal.

Biomass accumulation

TChl-a was integrated to 80 m depth, to the 0.415-mol m^{-2} d^{-1} isolume, and to the equivalent mixed layer depth h_{BD} (**Figure 9D**). The integration depth of 80 m was chosen because at that depth, chl-a concentrations in almost all profiles had come sufficiently close to 0 mg chl-a m^{-2} that no significant biomass was missed below (Figure S8.1, S8.2). It therefore represented the total biomass accumulation. As a considerable fraction of this biomass was located below the 0.415-mol m^{-2} d^{-1} isolume, not all of this biomass would contribute equally to primary production.

The phytoplankton TChl-a standing stock, whether integrated down to 80 m depth or the 0.415 isolume, peaked on average within 5–15 days of ice retreat at around 75 and 45 mg chl-a m^{-2}, respectively; the highest integrated biomass (0–80 m) encountered during the expedition was approximately 160 mg chl-a m^{-2} in ice-free waters (Figure S2.11). However, even at OWD = −20, 80-m integrated biomass was non-negligible at 40 mg chl-a m^{-2}. The under-ice TChl-a standing stock was thus below what has been measured in under-ice phytoplankton blooms by e.g., Assmy et al. (2017, 110–230 mg chl-a m^{-2}) or Arrigo et al. (2014, 300–1300 mg chl-a m^{-2}).

For hydrography and timing of biomass accumulation, our observations are largely consistent with the extensive literature on the physical and biological environment of the ice edge (e.g., Alexander and Niebauer, 1981; Sakshaug, 2004; Carmack and Wassmann, 2006; Wassmann and Reigstad, 2011) in two important regards: first, the MIZ, or transition from dense pack ice to open water, was rather narrow with high melt rates and low surface salinities leading to a shoaling of the mixing depth which coincided with increasing phytoplankton biomass; and second, the "bloom" (here, peak biomass) was a band of several kilometers width (Sakshaug et al., 1994) that followed the retreating ice edge on the open water side. Where these observations deviate from the classical picture is that neither the light field nor the vertical mixing seem to have prevented the bloom from starting much earlier, when the water was still ice-covered.

What constrained the under-ice bloom?

Euphotic zone and mixing depth

Our data indicate that light, amply sufficient for photosynthesis, penetrated the ice cover, and that stratification was not particularly weak; vertical mixing was presumably slow enough that the accumulation of biomass was not interrupted. With the euphotic zone extending below h_{BD}, the growth of phytoplankton cannot be expected to be disrupted by mixing out of the euphotic zone.

In addition, the biomass observed more than 50 km into the pack ice, at over 90% ice concentration, was unlikely to have been advected from more distant, less ice-covered waters. A quick dimensional analysis explains why. With open-ocean horizontal diffusivities typically of an order of magnitude around $O(1\ m^2\ s^{-1})$ (Manucharyan and Timmermans, 2013, chose 2 m^2 s^{-1} to study frontal dynamics), mixing over one day can be expected to occur at most on a scale of $\sqrt{K/1d} \sim O(100m)$. Because the ice retreated faster than that and only occasionally returned to a location where it had been a few days before (Figure S3.1), we can safely assume that the water sampled a few tens of kilometers into the MIZ was not advected from the ice-free side of the ice edge.

As all of our transects crossed between the Atlantic and Arctic domains, we consequently observed a deepening of the winter overturning depth towards larger OWD (**Figure 9**). Hence, the estimated pre-bloom surface nitrate concentration increased for OWD > −10, from around 5–6 μM to around 10 μM (Figures S6.1, S6.4). However, nitrate had not become limiting during our under-ice observations, and so we do not expect that the pre-bloom nitrate concentration explains the larger biomass in open water, even though we cannot exclude the possibility that the winter nutrient concentrations slightly modulated the observed phytoplankton standing stock.

Bloom timing

The above analysis means that some other factor or factors must have constrained the accumulation of under-ice biomass. Zooplankton grazing, viral lysis, and sinking may all have affected phytoplankton growth and thus limited the biomass accumulated under the ice, but these processes are beyond the scope of the current study. An inverse food web model suggests that in the western half of the station grid, 60–80% of NPP was grazed by secondary producers (B. Saint-Béat, personal communication), but we cannot say how this consumption may have been coupled temporally to phytoplankton growth.

Whatever the details of these phytoplankton loss terms, the bloom studied in this paper likely had been initiated at ice concentrations upward of 90%, more than ten days before the ice cover was gone. Bloom initiation would then have to be understood *sensu* Behrenfeld et al. (2017) as when phytoplankton growth exceeds loss terms due to an increase in light (with sufficient nutrient concentrations). In this scenario, phytoplankton loss terms could have lagged the increasing cell division rates, permitting biomass to accumulate until cell division rates peaked and loss terms caught up. Indeed, we observed that vertically integrated biomass increased in concert with the 3-m PAR irradiance, and reached its maximum when 3-m PAR irradiance plateaued from OWD > 5 (**Figure 9C** and **D**), after which nitrate depletion probably played a role in limiting phytoplankton growth. These issues deserve a follow-up study and more detailed treatment than can be given here.

Summary and Perspectives

In line with earlier investigations, we found Baffin Bay to be strongly segregated into two regimes which are mostly defined by the competing inflows of Atlantic and Arctic water masses. Winter overturning penetrated into the Atlantic water high-nutrient reservoir in the Atlantic sector, whereas in the Arctic sector it only reached the much less saline and hence nutrient-poorer Arctic waters that arrive from the Pacific Arctic through the Canadian Archipelago.

Because of the steady westward retreat of the ice edge through the study period, we could readily define and analyze the underwater light climate, vertical mixing, nutrient loading and chl-a distributions using a space-for-time approach, where the retreat speed served to link the number of open water days (OWD) to the distance from the moving ice edge. The timing and distribution of ice melt crucially influenced how the surface layer dynamics evolved.

Even at 90% ice cover and more than 10 days before the retreat of the ice from a given location, we observed all of the following (**Figure 9**): (1) nutrients were being consumed, as evidenced by the reduced, albeit not necessarily depleted, NO_3^- concentrations; (2) phytoplankton was growing, as evidenced by accumulating biomass; and (3) the euphotic zone extended below the surface layer defined by h_{BD}, i.e. the maximum extent of the mixing layer; vertical mixing did not likely constrain phytoplankton growth.

Wassmann (2011) depicted the ice-edge bloom in the "present" scenario as a highly localized feature that only appears once the optically impenetrable ice breaks apart. Our measurements of the rather deep 0.415 mol m^{-2} d^{-1} isolume, shallow vertical mixing, and considerable under-ice biomass indicate that the ice edge bloom was more spread out in time, congruent with the proposed "future" scenario (Wassmann, 2011, his **Figures 6C** and **7C**). A possible reason might be that the ice cover in Baffin Bay is predominantly seasonal, even over the strongly stratified Arctic Water (Tang et al., 2004), and hence much closer to the future seasonally ice covered Arctic Ocean than, e.g., the Barents Sea is (Loeng, 1991). Owing to phytoplankton growth under dense pack ice, the bloom studied in this paper may well have been initiated more than ten days before the ice cover retreated. In line with Behrenfeld et al. (2017), this early start could have happened by *increases* in irradiance, not necessarily the *amount* of irradiance, but further investigations are needed.

The phenological peak of the bloom (i.e., biomass accumulation) was not apparent until ten days after ice retreat. Although helpful for observing phytoplankton biomass and possibly primary production from space, this phenomenon might lead to incorrect conclusions about timing and constraining factors of the bloom when only the biomass peak is considered. As the Arctic sea ice cover becomes thinner (Kwok and Rothrock, 2009), entailing higher PAR transmittance (Nicolaus et al., 2012), higher melt rates and an earlier ice retreat, larger swaths of the Arctic Ocean may permit under-ice phytoplankton blooms, but as Lowry et al., 2014), suggested, these blooms might just have gone undetected for a much longer time before their relatively recent appraisal (see also Matrai and Apollonio, 2013). Our findings clearly demonstrate that in order to understand dynamics and constraints of Arctic ice edge blooms, we need to consider not only the in situ conditions sample by sample, but also the temporal coupling between them.

Data Accessibility Statement

All data are accessible at the Green Edge data base (http://www.obs-vlfr.fr/proof/php/GREENEDGE/greenedge.php) and will be made accessible after publication.

Supplemental files

The supplemental files for this article can be found as follows:

Acknowledgements

Competing interests

The authors have no competing interests to declare.

Author contributions

AR and MB led the design of the study. AR led the analysis and writing. AR made the figures, to which LO and LL contributed. AV and DD led sampling of the SCAMP data, which AV processed. MG ran the radiative transfer model and calculated surface irradiance of PAR. GB led acquisition and processing of the C-OPS irradiance data. JET and GD led sampling and processing of the nutrient samples. All authors contributed to the data analysis and writing.

References

Alexander, V and **Niebauer, HJ.** 1981. Oceanography of the Eastern Bering Sea Ice-Edge Zone in Spring. *Limnology and Oceanography* **26**(6): 1111–1125. ISSN 1939-5590. DOI: https://doi.org/10.4319/lo.1981.26.6.1111

Arrigo, KR, Perovich, DK, Pickart, RS, Brown, ZW, van Dijken, GL, Lowry, KE, Mills, MM, Palmer, MA, Balch, WM, Bates, NR, Benitez-Nelson, CR, Brownlee, E, Frey, KE, Laney, SR, Mathis, J, Matsuoka, A, Mitchell, BG, Moore, GWK, Reynolds, RA, Sosik, HM and **Swift, JH.** 2014. Phytoplankton Blooms beneath the Sea Ice in the Chukchi Sea. *Deep Sea Research Part II: Topical Studies in Oceanography* **105**: 1–16. ISSN 0967-0645. The Phytoplankton Megabloom beneath Arctic Sea Ice: Results from the ICESCAPE Program. DOI: https://doi.org/10.1016/j.dsr2.2014.03.018

Assmy, P, Fernández-Méndez, M, Duarte, P, Meyer, A, Randelhoff, A, Mundy, CJ, Olsen, LM, Kauko, HM, Bailey, A, Chierici, M, Cohen, L, Doulgeris, AP, Ehn, JK, Fransson, A, Gerland, S, Hop, H, Hudson, SR, Hughes, N, Itkin, P, Johnsen, G, King, JA, Koch, BP, Koenig, Z, Kwasniewski, S, Laney, SR, Nicolaus, M, Pavlov, AK, Polashenski, CM, Provost, C, Rösel, A, Sandbu, M, Spreen, G, Smedsrud, LH, Sundfjord, A, Taskjelle, T, Tatarek, A, Wiktor, J, Wagner, PM, Wold, A, Steen, H and **Granskog, MA.** 2017. Leads in Arctic Pack Ice Enable Early Phytoplankton Blooms below Snow-Covered Sea Ice. *Scientific Reports* **7**(40850). DOI: https://doi.org/10.1038/srep40850

Atlas, R, Hoffman, RN, Ardizzone, J, Leidner, SM, Jusem, JC, Smith, DK and **Gombos, D.** 2011. A Cross-Calibrated, Multiplatform Ocean Surface Wind Velocity Product for Meteorological and Oceanographic Applications. *Bulletin of the American Meteorological Society* **92**(2): 157–174. ISSN 0003-0007. DOI: https://doi.org/10.1175/2010BAMS2946.1

Behrenfeld, MJ. 2010. Abandoning Sverdrup's Critical Depth Hypothesis on Phytoplankton Blooms. *Ecology* **91**(4): 977–989. ISSN 0012-9658. DOI: https://doi.org/10.1890/09-1207.1

Behrenfeld, MJ and **Boss, ES.** 2017. Student's Tutorial on Bloom Hypotheses in the Context of Phytoplankton Annual Cycles. *Global Change Biology* **24**(1): 55–77. ISSN 1365-2486. DOI: https://doi.org/10.1111/gcb.13858

Behrenfeld, MJ, Hu, Y, O'Malley, RT, Boss, ES, Hostetler, CA, Siegel, DA, Sarmiento, JL, Schulien, J, Hair, JW, Lu, X, Rodier, S and **Scarino, AJ.** 2017. Annual Boom–Bust Cycles of Polar Phytoplankton Biomass Revealed by Space-Based Lidar. *Nature Geoscience* **10**(2): 118–122. ISSN 1752-0908. DOI: https://doi.org/10.1038/ngeo2861

Boss, E and **Behrenfeld, M.** 2010. In Situ Evaluation of the Initiation of the North Atlantic Phytoplankton Bloom. *Geophysical Research Letters* **37**(18). ISSN 00948276. DOI: https://doi.org/10.1029/2010GL044174

Bouffard, D and **Boegman, L.** 2013. A Diapycnal Diffusivity Model for Stratified Environmental Flows. *Dynamics of Atmospheres and Oceans* **61–62**: 14–34. ISSN 0377-0265. DOI: https://doi.org/10.1016/j.dynatmoce.2013.02.002

Brainerd, KE and **Gregg, MC.** 1995. Surface Mixed and Mixing Layer Depths. *Deep Sea Research Part I: Oceanographic Research Papers* **42**(9): 1521–1543. ISSN 0967-0637. DOI: https://doi.org/10.1016/0967-0637(95)00068-H

Carmack, EC. 2007. The Alpha/Beta Ocean Distinction: A Perspective on Fresh water Fluxes, Convection, Nutrients and Productivity in High-Latitude Seas. *Deep Sea Research Part II: Topical Studies in Oceanography* **54**: 2578–2598. DOI: https://doi.org/10.1016/j.dsr2.2007.08.018

Carmack, E and **Wassmann, P.** 2006. Food Webs and Physical – Biological Coupling on Pan-Arctic Shelves: Unifying Concepts and Comprehensive Perspectives. *Progress in Oceanography* **71**(2–4): 446–477. ISSN 0079-6611. DOI: https://doi.org/10.1016/j.pocean.2006.10.004

Cole, ST, Toole, JM, Rainville, L and **Lee, CM.** 2018. Internal Waves in the Arctic: Influence of Ice Concentration, Ice Roughness, and Surface Layer Stratification. *Journal of Geophysical Research: Oceans* ISSN 21699275. DOI: https://doi.org/10.1029/2018JC014096

Curry, B, Lee, CM, Petrie, B, Moritz, RE and **Kwok, R.** 2014. Multiyear Volume, Liquid Freshwater, and Sea Ice Transports through Davis Strait, 2004–10. *Journal of Physical Oceanography* **44**(4): 1244–1266. ISSN 0022-3670. DOI: https://doi.org/10.1175/JPO-D-13-0177.1

Cuypers, Y, Bouruet-Aubertot, P, Marec, C and **Fuda, JL.** 2012. Characterization of Turbulence from a Fine-Scale Parameterization and Microstructure Measurements in the Mediterranean Sea during the BOUM Experiment. *Biogeosciences* **9**(8): 3131–3149. ISSN 1726-4189. DOI: https://doi.org/10.5194/bg-9-3131-2012

Dewey, SR, Morison, JH and **Zhang, J.** 2017. An Edge-Referenced Surface Fresh Layer in the Beaufort Sea Seasonal Ice Zone. *Journal of Physical Oceanography* **47**(5): 1125–1144. DOI: https://doi.org/10.1175/JPO-D-16-0158.1

Ehn, JK, Mundy, CJ, Barber, DG, Hop, H, Rossnagel, A and **Stewart, J.** 2011. Impact of Horizontal Spreading on Light Propagation in Melt Pond Covered Seasonal Sea Ice in the Canadian Arctic. *Journal of Geophysical Research* **116**. ISSN 0148-0227. DOI: https://doi.org/10.1029/2010JC006908

Fissel, DB, Lemon, DD and **Birch, JR.** 1982. Major Features of the Summer Near-Surface Circulation of Western Baffin Bay, 1978 and 1979. *Arctic* **35**(1): 180–200. ISSN 0004-0843. DOI: https://doi.org/10.14430/arctic2318

Fortier, M, Fortier, L, Michel, C and **Legendre, L.** 2002. Climatic and Biological Forcing of the Vertical Flux of Biogenic Particles under Seasonal Arctic Sea Ice. *Marine Ecology Progress Series* **225**(1): 16. DOI: https://doi.org/10.3354/meps225001

Franks, PJS. 2015. Has Sverdrup's Critical Depth Hypothesis Been Tested? Mixed Layers vs. Turbulent Layers. *ICES Journal of Marine Science: Journal du Conseil* **72**(6): 1897–1907. ISSN 1054-3139, 1095-9289. DOI: https://doi.org/10.1093/icesjms/fsu175

Frey, KE, Perovich, DK and **Light, B.** 2011. The Spatial Distribution of Solar Radiation under a Melting Arctic Sea Ice Cover: SOLAR RADIATION UNDER ARCTIC SEA ICE. *Geophysical Research Letters* **38**(22). ISSN 00948276. DOI: https://doi.org/10.1029/2011GL049421

Geider, RJ, Osbonie, BA and **Raven, JA.** 1986. Growth, Photosynthesis and Maintenance Metabolic Cost in the Diatom Phaeodactylum Tricornutum at Very Low Light Levels. *Journal of Phycology* **22**(1): 39–48. ISSN 1529-8817. DOI: https://doi.org/10.1111/j.1529-8817.1986.tb02513.x

Grasshoff, K, Ehrhardt, M, Kremling, K and **Anderson, LG.** 1999. *Methods of Seawater Analysis.* 3rd, completely rev. and extended ed. Weinheim Wiley-VCH. ISBN 978-3-527-29589-0.

Gregg, M, D'Asaro, E, Riley, J and **Kunze, E.** 2018. Mixing Efficiency in the Ocean. *Annual Review of Marine Science* **10**(1): 443–473. DOI: https://doi.org/10.1146/annurev-marine-121916-063643

Guillot, P. 2016. CTD Data Collected by the CCGS Amundsen in the Canadian Arctic.

IOC, SCOR, IAPSO. 2010. The International Thermodynamic Equation of Sea-water – 2010: Calculation and Use of Thermodynamic Properties. Intergovernmental Oceanographic Commission, UNESCO.

Jakobsson, M, Mayer, L, Coakley, B, Dowdeswell, JA, Forbes, S, Fridman, B, Hodnesdal, H, Noormets, R, Pedersen, R, Rebesco, M, Schenke, HW, Zarayskaya, Y, Accettella, D, Armstrong, A, Anderson, RM, Bienhoff, P, Camerlenghi, A, Church, I, Edwards, M, Gardner, JV, Hall, JK, Hell, B, Hestvik, O, Kristoffersen, Y, Marcussen, C, Mohammad, R, Mosher, D, Nghiem, SV, Pedrosa, MT, Travaglini, PG and **Weatherall, P.** 2012. The International Bathymetric Chart of the Arctic Ocean (IBCAO) Version 3.0. *Geophysical Research Letters* **39**(12). ISSN 1944-8007. DOI: https://doi.org/10.1029/2012GL052219

Jones, EP, Anderson, LG and **Swift, JH.** 1998. Distribution of Atlantic and Pacific Waters in the Upper Arctic Ocean: Implications for Circulations. *Geophysical Research Letters* **25**(6): 765–768. ISSN 0094-8276. DOI: https://doi.org/10.1029/98GL00464

Katlein, C, Arndt, S, Nicolaus, M, Perovich, DK, Jakuba, MV, Suman, S, Elliott, S, Whitcomb, LL, McFarland, CJ, Gerdes, R, Boetius, A and **German, CR.** 2015. Influence of Ice Thickness and Surface Properties on Light Transmission through Arctic Sea Ice. *Journal of Geophysical Research: Oceans* **120**(9): 5932–5944. ISSN 21699275. DOI: https://doi.org/10.1002/2015JC010914

Kwok, R and **Rothrock, DA.** 2009. Decline in Arctic Sea Ice Thickness from Submarine and ICESat Records: 1958–2008. *Geophysical Research Letters* **36**(15). ISSN 1944-8007. DOI: https://doi.org/10.1029/2009GL039035

Lacour, L, Ardyna, M, Stec, KF, Claustre, H, Prieur, L, Poteau, A, D'Alcala, MR and **Iudicone, D.** 2017. Unexpected Winter Phytoplankton Blooms in the North Atlantic Subpolar Gyre. *Nature Geoscience* **10**(11): 836–839. ISSN 1752-0894, 1752-0908. DOI: https://doi.org/10.1038/ngeo3035

Laliberté, J, Bélanger, S and **Frouin, R.** 2016. Evaluation of Satellite-Based Algorithms to Estimate Photosynthetically Available Radiation (PAR) Reaching the Ocean Surface at High Northern Latitudes. *Remote Sensing of Environment* **184**: 199–211. ISSN 0034-4257. DOI: https://doi.org/10.1016/j.rse.2016.06.014

Letelier, RM, Karl, DM, Abbott, MR and **Bidigare, RR.** 2004. Light Driven Seasonal Patterns of Chlorophyll and Nitrate in the Lower Euphotic Zone of the North Pacific Subtropical Gyre. *Limnology and Oceanography* **49**(2): 508–519. ISSN 00243590. DOI: https://doi.org/10.4319/lo.2004.49.2.0508

Loeng, H. 1991. Features of the Physical Oceanographic Conditions of the Barents Sea. *Polar Research* **10**(1): 5–18. ISSN 1751-8369. DOI: https://doi.org/10.1111/j.1751-8369.1991.tb00630.x

Lowry, KE, van Dijken, GL and **Arrigo, KR.** 2014. Evidence of Under-Ice Phytoplankton Blooms in the Chukchi Sea from 1998 to 2012. *Deep Sea Research Part II: Topical Studies in Oceanography* **105**: 105–117. ISSN 0967-0645. DOI: https://doi.org/10.1016/j.dsr2.2014.03.013

Massicotte, P, Bécu, G, Lambert-Girard, S, Leymarie, E and **Babin, M.** 2018. Estimating Underwater Light Regime under Spatially Heterogeneous Sea Ice in the Arctic. *Applied Sciences* **8**(12): 2693. DOI: https://doi.org/10.3390/app8122693

Matrai, P and **Apollonio, S.** 2013. New Estimates of Microalgae Production Based upon Nitrate Reductions under Sea Ice in Canadian Shelf Seas and the Canada Basin of the Arctic Ocean. *Marine Biology* **160**(6): 1297–1309. ISSN 1432-1793. DOI: https://doi.org/10.1007/s00227-013-2181-0

McPhee, MG and **Kantha, LH.** 1989. Generation of Internal Waves by Sea Ice. *Journal of Geophysical Research: Oceans* **94**(C3): 3287–3302. ISSN 2156-2202. DOI: https://doi.org/10.1029/JC094iC03p03287

Morison, JH, McPhee, MG and **Maykut, GA.** 1987. Boundary Layer, Upper Ocean, and Ice Observations in the Greenland Sea Marginal Ice Zone. *Journal of Geophysical Research: Oceans* **92**(C7): 6987–7011. ISSN 2156-2202. DOI: https://doi.org/10.1029/JC092iC07p06987

Münchow, A, Falkner, KK and **Melling, H.** 2015. Baffin Island and West Greenland Current Systems in Northern Baffin Bay. *Progress in Oceanography* **132**: 305–317. ISSN 0079-6611. DOI: https://doi.org/10.1016/j.pocean.2014.04.001

Mundy, CJ, Gosselin, M, Ehn, J, Gratton, Y, Rossnagel, A, Barber, DG, Martin, J, Tremblay, J-É, Palmer, M, Arrigo, KR, Darnis, G, Fortier, L, Else, B and **Papakyriakou, T.** 2009. Contribution of Under-Ice Primary Production to an Ice-Edge Upwelling Phytoplankton Bloom in the Canadian Beaufort Sea. *Geophysical Research Letters* **36**(17). ISSN 0094-8276. DOI: https://doi.org/10.1029/2009GL038837

Newton, R, Schlosser, P, Mortlock, R, Swift, J and **MacDonald, R.** 2013. Canadian Basin Freshwater Sources and Changes: Results from the 2005 Arctic Ocean Section. *Journal of Geophysical Research: Oceans* **118**(4): 2133–2154. DOI: https://doi.org/10.1002/jgrc.20101

Nicolaus, M, Katlein, C, Maslanik, J and **Hendricks, S.** 2012. Changes in Arctic Sea Ice Result in Increasing Light Transmittance and Absorption. *Geophysical Research Letters* **39**(24). ISSN 1944-8007. DOI: https://doi.org/10.1029/2012GL053738

Osborn, TR. 1980. Estimates of the Local Rate of Vertical Diffusion from Dissipation Measurements. *J Phys Oceanogr* **10**(1): 83–89. ISSN 0022-3670. DOI: https://doi.org/10.1175/1520-0485(1980)010<0083:EOTLRO>2.0.CO;2

Oziel, L, Massicotte, P, Randelhoff, A, Ferland, J, Vladoiu, A, Lacour, L, Galindo, V, Lambert-Girard, S, Dumont, D, Cuypers, Y, Bouruet-Aubertot, P, Mundy, CJ, Ehn, J, Bécu, G, Marec, C, Forget, M-H, Garcia, N, Coupel, P, Raimbault, P, Houssais, M-N and **Babin, M.** 2019. Environmental Factors Influencing the Seasonal Dynamics of Under-Ice Spring Blooms in Baffin Bay. *Submitted to Elem Sci Anth.*

Pavlov, AK, Taskjelle, T, Kauko, HM, Hamre, B, Hudson, SR, Assmy, P, Duarte, P, **Fernández-Méndez, M, Mundy, CJ** and **Granskog, MA.** 2017. Altered Inherent Optical Properties and Estimates of the Underwater Light Field during an Arctic Under-Ice Bloom of Phaeocystis Pouchetii. *Journal of Geophysical Research: Oceans* **122**(6): 4939–4961. ISSN 2169-9291. DOI: https://doi.org/10.1002/2016JC012471

Peralta-Ferriz, C and **Woodgate, RA.** 2015. Seasonal and Interannual Variability of Pan-Arctic Surface Mixed Layer Properties from 1979 to 2012 from Hydrographic Data, and the Dominance of Stratification for Multiyear Mixed Layer Depth Shoaling. *Progress in Oceanography* **134**: 19–53. ISSN 0079-6611. DOI: https://doi.org/10.1016/j.pocean.2014.12.005

Perovich, DK and **Polashenski, C.** 2012. Albedo Evolution of Seasonal Arctic Sea Ice: ALEDO EVOLUTION OF SEASONAL SEA ICE. *Geophysical Research Letters* **39**(8). ISSN 00948276. DOI: https://doi.org/10.1029/2012GL051432

Perrette, M, Yool, A, Quartly, GD and **Popova, EE.** 2011. Near-Ubiquity of Ice-Edge Blooms in the Arctic. *Biogeosciences* **8**(2): 515–524. ISSN 1726-4189. DOI: https://doi.org/10.5194/bg-8-515-2011

Randelhoff, A, Fer, I and **Sundfjord, A.** 2017. Turbulent Upper-Ocean Mixing Affected by Meltwater Layers during Arctic Summer. *Journal of Physical Oceanography* **47**(4): 835–853. DOI: https://doi.org/10.1175/JPO-D-16-0200.1

Randelhoff, A, Fer, I, Sundfjord, A, Tremblay, JE and **Reigstad, M.** 2016. Vertical Fluxes of Nitrate in the Seasonal Nitracline of the Atlantic Sector of the Arctic Ocean. *Journal of Geophysical Research: Oceans* **121**(7): 5282–5295. ISSN 2169-9291. DOI: https://doi.org/10.1002/2016JC011779

Randelhoff, A, Oziel, L, Massicotte, P, Bécu, G, Galí, M, Lacour, L, Dumont, D, Vladoiu, A, Marec, C, Bruyant, F, Houssais, M-N, Tremblay, J-E, Deslongchamps, G and **Babin, M.** 2019. Code and Data for: The Evolution of Light and Vertical Mixing across a Phytoplankton Ice-Edge Bloom. DOI: https://doi.org/10.5281/zenodo.2653854

Randelhoff, A, Sundfjord, A and **Reigstad, M.** 2015. Seasonal Variability and Fluxes of Nitrate in the Surface Waters over the Arctic Shelf Slope. *Geophysical Research Letters* **42**(9): 3442–3449. ISSN 0094-8276. DOI: https://doi.org/10.1002/2015GL063655

Ras, J, Claustre, H and **Uitz, J.** 2008. Spatial Variability of Phytoplankton Pigment Distributions in the Subtropical South Pacific Ocean: Comparison between in Situ and Predicted Data. *Biogeosciences* **5**(2): 353–369. ISSN 1726-4189. DOI: https://doi.org/10.5194/bg-5-353-2008

Ricchiazzi, P, Yang, S, Gautier, C and **Sowle, D.** 1998. SBDART: A Research and Teaching Software Tool for Plane-Parallel Radiative Transfer in the Earth's Atmosphere. *Bulletin of the American Meteorological Society* **79**(10): 2101–2114. ISSN 0003-0007. DOI: https://doi.org/10.1175/1520-0477(1998)079<2101:SARATS>2.0.CO;2

Ruddick, BR, Anis, A and **Thompson, K.** 2000. Maximum Likelihood Spectral Fitting: The Batchelor Spectrum. *Journal Of Atmospheric And Oceanic Technology* **17**: 15. DOI: https://doi.org/10.1175/1520-0426(2000)017<1541:MLSFTB>2.0.CO;2

Rudels, B, Anderson, LG and **Jones, EP.** 1996. Formation and Evolution of the Surface Mixed Layer and Halocline of the Arctic Ocean. *Journal of Geophysical Research: Oceans* **101**(C4): 8807–8821. ISSN 2156-2202. DOI: https://doi.org/10.1029/96JC00143

Sakshaug, E. 2004. Primary and Secondary Production in the Arctic Seas. In: Stein, R and MacDonald, R (eds.), *The Organic Carbon Cycle in the Arctic Ocean*, 57–81. Berlin, Heidelberg: Springer. ISBN 978-3-642-62351-6. DOI: https://doi.org/10.1007/978-3-642-18912-8

Sakshaug, E, Bjørge, A, Gulliksen, B, Loeng, H and **Mehlum, F.** 1994. Structure, Biomass Distribution, and Energetics of the Pelagic Ecosystem in the Barents Sea: A Synopsis. *Polar Biology* **14**(6): 405–411. ISSN 1432-2056. DOI: https://doi.org/10.1007/BF00240261

Schmidtko, S, Johnson, GC and **Lyman, JM.** 2013. MIMOC: A Global Monthly Isopycnal Upper-Ocean Climatology with Mixed Layers: MIMOC. *Journal of Geophysical Research: Oceans* **118**(4): 1658–1672. ISSN 21699275. DOI: https://doi.org/10.1002/jgrc.20122

Shih, LH, Koseff, JR, Ivey, GN and **Ferziger, JH.** 2005. Parameterization of Turbulent Fluxes and Scales Using Homogeneous Sheared Stably Stratified Turbulence Simulations. *Journal of Fluid Mechanics* **525**: 193–214. ISSN 0022-1120, 1469-7645. DOI: https://doi.org/10.1017/S0022112004002587

Spreen, G, Kaleschke, L and **Heygster, G.** 2008. Sea Ice Remote Sensing Using AMSRE 89-GHz Channels. *Journal of Geophysical Research* **113**(C2): C02S03. ISSN 0148-0227. DOI: https://doi.org/10.1029/2005JC003384

Steele, M and **Ermold, W.** 2015. Loitering of the Retreating Sea Ice Edge in the Arctic Seas. *Journal of Geophysical Research: Oceans* **120**(12): 7699–7721. ISSN 2169-9291. DOI: https://doi.org/10.1002/2015JC011182

Tang, CC, Ross, CK, Yao, T, Petrie, B, DeTracey, BM, et al. 2004. The Circulation, Water Masses and Sea-Ice of Baffin Bay. *Progress in Oceanography* **63**(4): 183–228. ISSN 0079-6611. DOI: https://doi.org/10.1016/j.pocean.2004.09.005

Torres-Valdés, S, Tsubouchi, T, Bacon, S, Naveira-Garabato, AC, Sanders, R, et al. 2013. Export of Nutrients from the Arctic Ocean. *J Geophys Res Oceans* **118**(4): 1625–1644. ISSN 2169-9275. DOI: https://doi.org/10.1002/jgrc.20063

Tremblay, JE, Anderson, LG, Matrai, P, Coupel, P, Bélanger, S, et al. 2015. Global and Regional Drivers of Nutrient Supply, Primary Production and CO2 Drawdown in the Changing Arctic Ocean. *Progress in Oceanography* **139**: 171–196. ISSN 0079-6611. DOI: https://doi.org/10.1016/j.pocean.2015.08.009

Wassmann, P. 2011a. Arctic Marine Ecosystems in an Era of Rapid Climate Change. *Progress in Oceanography* **90**(1): 1–17. ISSN 0079-6611. DOI: https://doi.org/10.1016/j.pocean.2011.02.002

Wassmann, P and **Reigstad, M.** 2011b. Future Arctic Ocean Seasonal Ice Zones and Implications for Pelagic-Benthic Coupling. *Oceanography* **24**(3): 220–231. ISSN 10428275, 2377617X. DOI: https://doi.org/10.5670/oceanog.2011.74

Woodgate, RA, Aagaard, K, Swift, JH, Falkner, KK and **Smethie, WM.** 2005. Pacific Ventilation of the Arctic Ocean's Lower Halocline by Upwelling and Diapycnal Mixing over the Continental Margin. *Geophysical Research Letters* **32**(18). ISSN 1944-8007. DOI: https://doi.org/10.1029/2005GL023999

Zweng, MM and **Münchow, A.** 2006. Warming and Freshening of Baffin Bay, 1916–2003. *Journal of Geophysical Research* **111**(C7): C07016. ISSN 0148-0227. DOI: https://doi.org/10.1029/2005JC003093